ACS Catalysis

Perspective

Cite This: ACS Catal. 2019, 9, 920−931

pubs.acs.org/acscatalysis

Challenges in Modeling Electrochemical Reaction Energetics with Polarizable Continuum Models

Joseph A. Gauthier,[†,‡] Stefan Ringe,[‡,†] Colin F. Dickens,[†,‡] Alejandro J. Garza,[¶] Alexis T. Bell,[¶,§,#] Martin Head-Gordon,[¶,∥,#] Jens K. Nørskov,[†,‡] and Karen Chan*[,‡]

[†]SUNCAT Center for Interface Science and Catalysis, Department of Chemical Engineering, Stanford University, Stanford, California 94305, United States

[‡]SUNCAT Center for Interface Science and Catalysis, SLAC National Accelerator Laboratory, 2575 Sand Hill Road, Menlo Park, California 94025, United States

[¶]The Joint Center for Artificial Photosynthesis, Lawrence Berkeley National Laboratory, Berkeley California 94720, United States

[§]Department of Chemical and Biomolecular Engineering, University of California at Berkeley, Berkeley, California 94720, United States

[∥]Department of Chemistry, University of California at Berkeley, Berkeley, California 94720, United States

[#]Chemical Sciences Division, Lawrence Berkeley National Laboratory, Berkeley, California 94720, United States

Supporting Information

ABSTRACT: A major challenge in the modeling of electrochemical phenomena is the accurate description of the interface between an electrolyte and a charged conductor. Polarizable continuum models (PCM) have been gaining popularity because they offer a computationally inexpensive method of modeling the electrolyte. In this Perspective, we discuss challenges from using one such model which treats the ions using a linearized Poisson−Boltzmann (LPB) distribution. From a physical perspective, this model places charge unphysically close to the surface and adsorbates, and it includes excessively steep ramping of the dielectric constant from the surface to the bulk solvent. Both of these issues can be somewhat mitigated by adjusting parameters built into the model, but in doing so, the resultant capacitance deviates from experimental values. Likewise, hybrid explicit-implicit approaches to the solvent may offer a more realistic description of hydrogen bonding and solvation to reaction intermediates, but the corresponding capacitances also deviate from experimental values. These deviations highlight the need for a careful adjustment of parameters in order to reproduce not only solvation energies but also other physical properties of solid−liquid interfaces. Continuum approaches alone also necessarily do not capture local variations in the electric field from cations at the interface, which can affect the energetics of intermediates with substantial dipoles or polarizability. Finally, since the double-layer charge can be varied continuously, LPB/PCM models provide a way to determine electrochemical barriers at constant potential. However, double-layer charging and the atomic motion associated with reaction events occur on significantly different timescales. We suggest that more detailed approaches, such as the modified Poisson−Boltzmann model and/or the addition of a Stern layer, may be able to mitigate some but not all of the challenges discussed.

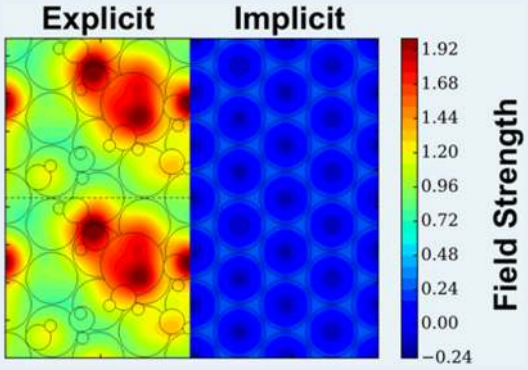

KEYWORDS: *density functional theory, catalysis, electrocatalysis, electrochemistry, solvation*

1. INTRODUCTION

The interface between an electrode and the surrounding electrolyte plays a central role in electrochemistry, yet our understanding of its structure and function is still limited. Historically, theories have adopted a continuum description of the ions and treat the solvent as a dielectric medium.[1−6] Such models have offered insight into the ion distribution of the double layer and the charging behavior of the interface. In recent ab initio investigations of electrochemical reaction energetics, there are two main approaches toward the electrolyte: a fully explicit, atomistic description, or an implicit description that builds upon classical continuum models.

In principle, a fully explicit description of the electrolyte would provide the most accurate description of the effects of solvation, interfacial fields, and applied bias.[7−15] However, an explicit description of the electrolyte is computationally demanding, and current approaches can often not appropri-

Received: July 16, 2018
Revised: November 20, 2018
Published: November 28, 2018

DOI: 10.1021/acscatal.8b02793
ACS Catal. 2019, 9, 920−931

ately sample the solvent's phase space at the desired thermodynamic conditions.[8,12,16−20] While it is possible in principle to adequately sample the solvent and ionic configuration space with a fully explicit approach,[21,22] such studies are extremely computationally demanding and not practical for the analysis of complex reaction mechanisms or for materials screening. Furthermore, achieving constant electrode potential during MD runs via the implementation of a potentiostat is technically challenging and requires the use of a continuum charge description to express noninteger fluctuations of the counter-charge density,[23] which poses several challenges as we discuss below. Explicitly modeled water can also suffer from band misalignment as reported in ref 24, because of poor description of the solvent LUMO and HOMO levels, and the resultant gap. This can in some cases result in unphysical charge transfer between the solvent and metal.

Implicit models, on the other hand, model the electrolyte using continuum approaches. Although such models have been developed for a long time, it is, to date, still unclear to what extent these methods accurately describe electrocatalytic processes at solid−liquid interfaces. Several types of implicit models have been proposed: a homogeneous background charge in the entire model system,[25−27] a Gaussian counter-charge distribution outside the surface,[28,29] and, more recently, a Poisson−Boltzmann description of the solvent and ion distribution.[30−38] The last approach is available in several widely used electronic structure codes[30,32,34,39−41] and has been successfully applied in a number of recent mechanistic studies of oxygen evolution, CO_2 reduction, and CO reduction.[42−47] By utilizing Green's function techniques to lift the requirement of periodicity in the direction normal to the surface, compensating charge can be modeled as an effective screening medium.[48,49] These techniques have been applied to surfaces to eliminate spurious multipole interactions associated with DFT slab calculations,[50] and as part of a scheme for grand-canonical ab initio molecular dynamics.[23] Several approaches combine quantum-level DFT with classical DFT for the electrolyte.[45,51−53] Finally, implicit continuuml atomistic hybrids, dubbed microsolvation,[15] present the possibility of a computationally inexpensive solution by including a minimal amount of explicit solvent molecules within a continuum model framework. Such an approach avoids the elaborate calculations needed for explicit inclusion of solvent and ions, while retaining an ab initio consideration of the effect of solvent and ions at the interface.[9,15,42−44,54,55]

A particular challenge in ab initio computational electrocatalysis is the need for the inclusion of applied bias at the electrode. At the most basic level, an applied bias improves the feasibility of the overall process by shifting the energetics of each oxidative or reductive step in the process. This effect of the applied bias on the reaction thermodynamics is captured in the computational hydrogen electrode (CHE) model at effectively zero additional computational cost relative to surface science calculations, and represents a very simple and still widely used model applied to electrocatalysis.[56] While the CHE in principle can be[12,17,57] applied in conjunction with solvent and external electric fields, it cannot alone be used to probe charge transfer barriers and the associated kinetics.[58]

Because fully explicit solvent models operate under a constant number of electrons, changes in the dipole of the interface from either chemical or electrochemical steps along the reaction barrier lead to corresponding shifts in potential, and extrapolation methods are needed to bridge the constant charge and constant potential limits.[20,58] Implicit solvent-electrolyte methods, which allow for a continuous variation of interfacial charge, offer the possibility of simulations at constant potential, since the Fermi level can be matched to the desired bias in an iterative manner. Due to the implicit solvent and electrolyte, it preserves the advantage of low-dimensional potential surfaces and avoids the need for statistical mechanics, and therefore requires a computational cost increase of only several-fold relative to bias-free modeling. For these reasons, the variants of this approach are likely to be widely used in the near future.

In the present Perspective, we examine the combined linearized Poisson−Boltzmann/polarizable continuum model (LPB/PCM)-DFT method and discuss a number of associated open challenges. We investigate the resultant charge distribution at the electrochemical interface and show how it affects the energetics of two elementary processes, CO_2 adsorption, and the Volmer reaction on Pt(111). In particular, we discuss several challenges associated with the determination of the electrochemical interfacial structure and reaction energetics:

1. Default parametrizations place the ionic countercharge unphysically close to the metal surface, and the dielectric constants are ramped too quickly to the bulk values.
2. LPB/PCM models alone cannot capture the local field variations from explicit cations.
3. Hybrid explicit/implicit descriptions of water lead to deviations in interfacial capacitance from experimental values and unphysical spilling of continuum counter-charge into Ångström-sized regions between explicit solvent molecules.
4. Constant potential reaction energetics are determined under the assumption that ion and solvent reorganization follow adiabatically the atomic motion associated with a reaction event. While this charging response gives rise to constant potential conditions, it also leads to variations in surface charge density and electric field along the reaction pathway.

2. THEORETICAL METHODS AND MODEL DETAILS

The results presented in this work are based on density functional theory (DFT) calculations performed with the Vienna ab initio Simulation Package[59−61] in conjunction with VASPsol,[32,39] but the conclusions presented herein are generally not specific to this implementation. Core electrons of each atom were modeled with projector augmented wave pseudopotentials,[62] while valence electrons were expanded as plane-waves up to a kinetic energy cutoff of 500 eV. When optimizing bulk platinum, the Brillouin zone was sampled with a 12 × 12 × 12 Γ-centered Monkhorst−Pack[63] k-point grid, with valence electrons described by a plane-wave expansion up to 500 eV. Exchange and correlation interactions were accounted for using the RPBE functional for the CO_2 data[64] and the PBE functional for the Volmer data.[65] The accuracy of predicted solvation effects depends on the functional which was used to parametrize the implicit solvation model.[39] However, the transferability of the parameters to RPBE has been demonstrated.[43] RPBE was then chosen for the study of CO_2 adsorption for its improved accuracy in estimating chemisorption energies.[64,66] PBE was chosen for the Volmer study for its more accurate description of water geometries.[67]

DOI: 10.1021/acscatal.8b02793
ACS Catal. 2019, 9, 920−931

We did not include any van der Waals corrections to avoid any possible solvation uncertainties due to the risk of non-transferability of the implicit solvation parameters.

Surface CO_2 calculations were performed on a 4 × 4 supercell, with four layers of surface atoms; the outer two layers were free to relax, while the middle two were constrained to the bulk lattice parameter of a = 3.989 Å. These supercells were symmetric in the z-coordinate to prevent any net dipole interaction. We note that because the continuum solvation screens any net dipole (meaning the use of the dipole correction[68] is unnecessary), using a symmetric cell in the z-coordinate seems to have a negligible effect on the overall reaction energetics, as seen in SI Figure S1. Volmer calculations were performed in a 4 × 3 supercell, with three layers of surface atoms; the uppermost layer was free to relax, and the lower two layers were frozen to the bulk lattice parameter of a = 3.967 Å. This slightly smaller lattice parameter is due to the different exchange-correlation functional used for the Volmer calculations. One explicit bilayer of solvent (8 water molecules) was included.

Geometries were considered optimized when the maximum force on any atom in the system was below 0.03 eV $Å^{-1}$. For each electronic self-consistency cycle, the electronic energy was considered converged when it did not change by more than 10^{-4} eV between iterations.

VASPsol treats solvent at the electrochemical interface implicitly (i.e., as a polarizable dielectric continuum described by the isotropic dielectric permittivity function ε). The ionic counter charge density ρ_{ion} is modeled by the linearized Poisson−Boltzmann (LPB) approach (given in atomic units):[32,39]

$$\rho_{ion}(\mathbf{x}) = -\mathcal{S}(\tilde{\rho}_{el}(\mathbf{x}))\left(\frac{2c^0(qz)^2}{k_bT}\right)\phi(\mathbf{x}) = -\kappa^2(\tilde{\rho}_{el}(\mathbf{x}))\phi(\mathbf{x}) \tag{1}$$

where c^0 is the ion concentration in the bulk solvent, q is the elementary charge, z the magnitude of the ionic charge, k_b the Boltzmann constant, T the temperature, and $\phi(\mathbf{x})$ the electrostatic potential being the solution of the LPB equation:

$$[\nabla\cdot\{\varepsilon(\tilde{\rho}_{el}(\mathbf{x}))\nabla\}]\phi(\mathbf{x}) = -4\pi(\rho_{el}(\mathbf{x}) + \rho_{nuc}(\mathbf{x}) + \rho_{ion}(\mathbf{x})) \tag{2}$$

$\tilde{\rho}_{el}(\mathbf{x})$ is the valence electron density plus a Gaussian pseudocore charge density, added at the nuclei to avoid solvent leakage inside of the atoms where the valence charge density can be small. $\rho_{el}(\mathbf{x})$ is the valence electron density resulting from Kohn−Sham (KS) DFT, and $\rho_{nuc}(\mathbf{x})$ is the nuclear charge density modeled as Gaussians.

To describe the interface between the electrode and electrolyte, both κ (cf. eq 1) and ε are ramped up from inside the surface to the polarizable continuum by the shape function $\mathcal{S}$:

$$\varepsilon(\tilde{\rho}_{el}(\mathbf{x})) = 1 + (\varepsilon_b - 1)(\mathcal{S}(\tilde{\rho}_{el}(\mathbf{x})) \tag{3}$$

with

$$\mathcal{S}(\tilde{\rho}_{el}(\mathbf{x})) = \frac{1}{2}\mathrm{erfc}\left[\frac{\log\left(\frac{\tilde{\rho}_{el}(\mathbf{x})}{\tilde{\rho}_{el,cut}}\right)}{\sigma\sqrt{2}}\right] \tag{4}$$

As in many implicit solvation models,[30,33,38] the solute's valence electron density is used to define the dielectric transition from solute (ε = 1) to bulk solvent ($\varepsilon = \varepsilon_b$). Analogously, the ion exclusion function κ, which models ion−solute repulsions, is ramped up from 0 to κ_b, the inverse Debye length. The above functional form of $\mathcal{S}$ gives rise to two parameters determining the solvation and ion effect, an electron density cutoff $\tilde{\rho}_{el,cut}$ and a smoothness parameter σ.

Nonelectrostatic contributions to solvation such as cavitation and repulsion are described by adding to the electrostatic KS energy expression the empirical term,[69]

$$A_{cav} = \tau\int|\nabla\mathcal{S}|\mathrm{d}^3\mathbf{x} \tag{5}$$

where the integral over the gradient of $\mathcal{S}$ is a representation of the surface area of the solvation cavity, and τ can be considered as effective surface tension parameter which describes the nonelectrostatic interactions. Further details on the implementation of this model can be found in references 32 and 39.

To summarize, the ion distribution is determined by the five constants ε_b, κ_b, $\tilde{\rho}_{el,cut}$, σ, and τ. Default parameters for VASPsol are 78.4, 0.0 $Å^{-1}$, 2.5 × 10^{-3} $Å^{-3}$, 0.6, and 5.25 × 10^{-4} eV $Å^{-2}$, respectively, and were determined through fits to known experimental hydration energies of organic molecules.[39]

In contrast to the case of molecular solutes, where the parametrization against experimentally measured solvation energies has been shown to lead to reliable and transferable models,[30,32−34,53,69−71] this has not yet been proven for the case of extended surface slabs. The default parameters have been shown to give reasonable capacitances and potentials of zero charges (PZCs) on single-crystal transition-metal surfaces.[32,35,39,43,72] We note also that the PZC and surface work functions of metal slabs are linearly correlated,[73] so an accurate PZC prediction may be more reflective of the atomistic description of the metal work function than the description of the electrolyte. Furthermore, it is not clear that a correct description of pure metal surface properties in solution gives transferable estimates of solvation effects and reaction energies of arbitrary adsorbates. Recently, it was shown in implicit models for molecular solvation that ion-specific solute-ion repulsions can be correlated to differences in charge density cutoffs for these functions.[70] Therefore, assuming the availability of accurate experimental reference data, a careful parametrization of density cutoffs may enable modeling ion-specific capacitances on extended surfaces.

Due to the numerical instabilities illustrated in Supporting Information (SI) Figure S2, τ is set to 0 for all calculations in this work, except where specified, as has been done in previous studies.[71,74] Table 1 shows the effects of varying ε_b, $\tilde{\rho}_{el,cut}$, and τ on the overall capacitance (C) and PZC, and the corresponding surface charge density vs potential curves used to determine C and PZC are shown in Figure S3 in the SI. Table 1 shows that the shift from the default value to 0 gives slight shifts in both capacitance and PZC. The effects of the variations in ε_b and τ are discussed further below, and a more complete factorial experiment showing the parameter dependence of PZC is shown in SI Figure S4.

Because of the adsorption of hydrogen and oxygen species, the experimental value for the PZC of Pt(111) has a large uncertainty, with reported values between 0.2 to 1.1 V vs SHE.[75,76] This scatter motivates the development of more reliable theoretical predictions of the PZC. A parity comparison between calculated and experimental reference

DOI: 10.1021/acscatal.8b02793
ACS Catal. 2019, 9, 920−931

Table 1. Tabulated Capacitances and Potentials of Zero Charge of Pt(111) for Varying Levels of Bulk Dielectric Constant ϵ_b, Effective Surface Tension τ, and Electron Density Cutoff $\tilde{\rho}_{el,cut}$[a]

ϵ_b	$\tilde{\rho}_{el,cut}$/Å^{-3}	τ/meV Å^{-2}	C/μF cm^{-2}	PZC/V vs SHE
78.4	2.5×10^{-3}	0.525	15.1	0.9
78.4	2.5×10^{-3}	0.0	13.7	1.0
78.4	1.0×10^{-6}	0.0	3.4	1.2
4.0	2.5×10^{-3}	0.525	5.7	1.0
4.0	2.5×10^{-3}	0.0	5.4	1.1
4.0	1.0×10^{-6}	0.0	2.7	1.2

[a]In all cases, σ = 6.0, and $\kappa_b = \frac{1}{3}$Å^{-1}. Row 1 shows the results for the default parameters.

values for various transition metals[75,76] is shown in SI Figure S5.

Reaction energies at constant electrode potential were calculated using an implementation similar to the method of ref 43. The electrode potential is given by eq 6.[31]

$$U_{SHE}(n) = \frac{-\epsilon_F(n) - \phi_{SHE}}{e} \tag{6}$$

Here ϕ_{SHE} is the work function of the Standard Hydrogen Electrode, determined experimentally to be 4.4 eV,[77] and ϵ_F is the Fermi energy of the slab relative to vacuum. A fixed-point iteration scheme was added to the KS DFT self-consistent field scheme, where the number of electrons n in the system was varied to reach the desired U_{SHE}. Using Newton's Method, we minimize $\tilde{U}_{SHE}(n)$,

$$\min_n \tilde{U}_{SHE}(n) = \min_n |U_{SHE}(n) - U_{des}| \tag{7}$$

where $U_{SHE}(n)$ is the electrode potential at n electrons, and U_{des} the desired potential.

In practice, Newton's Method generally takes only three SCF cycles to converge to the correct charge, since ϵ_F depends approximately linearly on n. The optimization of n is followed by a geometry optimization step. This process repeated until both the geometry is optimized to the aforementioned criteria and the potential is within 0.02 V of the desired potential.

The grand-canonical free energy of a reaction is obtained by accounting for the electronic and ionic reservoir energies being in exchange with the modeled system,[43]

$$\Delta\Omega = \Delta G - \mu_{e^-}(N_{e^-}^{FS} - N_{e^-}^{IS}) \tag{8}$$

Here, ΔG represents the change in Gibbs free energy required for an unsolvated CO_2 molecule to adsorb to a charged, solvated surface, containing the typical vibrational and zero point energies. The free energy of the reference reservoir of electrons, μ_{e^-}, is taken to be the Fermi energy corresponding to the desired potential and $N_{e^-}^{FS}$ and $N_{e^-}^{IS}$ denote the total number of electrons in the final and initial state, respectively.

We examined the convergence of the adsorption energy of CO_2 on Pt(111) with respect to the separation between periodic slabs, as illustrated in SI Figure S6. We note that, due to the extent of the ion distribution, a separation between slabs of at least 50 Å is required to obtain adsorption energies within 0.1 eV of the infinite vacuum limit using default parameters. This issue seems to be related to long-range interactions between the repeated slabs, where we found the adsorption energy to follow a nearly perfect inverse cell volume dependence (cf. SI Figure S5). This decay length is proportional to the Debye length, meaning that for larger Debye lengths, even larger vacuum separations are necessary, as was found in ref 44. Despite the applicability of the linearized Poisson−Boltzmann equation to a very limited region near the PZC, such a model has been widely applied to study electrochemical reactions within potential ranges of ±0.5 V, which we investigate in this work.

3. RESULTS AND DISCUSSION

Here we discuss several challenges identified with the use of LPB/PCM for understanding electrochemical reaction energetics. We first discuss those associated with physical description of the solvent and ion distribution, followed by those related to the determination of reaction energetics under constant potential.

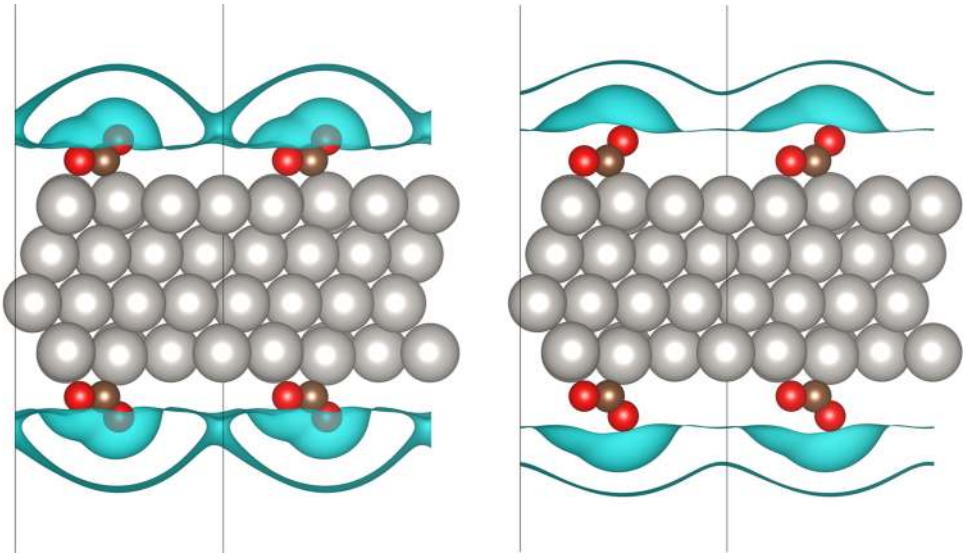

Figure 1. Ionic countercharge density isosurfaces of 2×10^{-3} eÅ^{-3} for CO_2 adsorbed on Pt(111) in a 2 × 4 supercell. Left: Default $\tilde{\rho}_{el,cut} = 2.5 \times 10^{-3}$ eÅ^{-3}. Right: Lowered $\tilde{\rho}_{el,cut} = 1.0 \times 10^{-6}$ eÅ^{-3}.

DOI: 10.1021/acscatal.8b02793
ACS Catal. 2019, 9, 920−931

3.1. Description of the Solvent and the Ion Distribution. *3.1.1. Ionic Countercharge Placement.* The LPB/PCM model as introduced above applies the same ramping function for ionic charge density and permittivity. Using default parameters and a Debye length of 3 Å, this leads to ions being placed unphysically close to the metal surface. The reason for this is a nonoptimal parametrization of the ionic shape function using the same cutoff parameter as for the dielectric ramping. In reality, ions are separated from the electrode by an effective hydration shell and physisorbed water, an effect that can be modeled by shifting the onset of the ion distribution further away from the surface.[70]

Figure 1 (left) illustrates a counter-charge density isosurface of 2×10^{-3} eÅ^{-3} (corresponding to a value near the maximum density) on a *CO_2 | Pt(111) system using the default $\tilde{\rho}_{el,cut}$. Here the counter-charge is placed within 2 Å of the surface. Explicit solvent simulations suggest cations to be placed roughly 3−5 Å from the surface,[6,78] due to the size of the solvation shells of the ions. By adjusting $\tilde{\rho}_{el,cut}$ from the default value of 2.5×10^{-3} Å^{-3} to the much lower value of 1.0×10^{-6} Å^{-3}, we can move the counter-charge density to a more physical location, as seen in Figure 1 (right), with almost enough room for an explicit water layer. The isosurface being multivalued in the z-coordinate arises from the rapid rise and subsequent decay of ion concentration moving away from the surface.

However, when the countercharge density is pushed away, the model's ability to predict the capacitance of Pt(111) is lost. As shown in Table 1 (and SI Figure S4), we observe a significant decrease (from 13.7 μF cm^{-2} to 3.4 μF cm^{-2}) in the predicted capacitance relative to the capacitance reported in the model reference,[32,39] and significantly lower than experimentally determined.[79] The sensitivity of the capacitance to $\tilde{\rho}_{el,cut}$ is in-line with the explorations on the Li | PCM interface reported in ref 80. We note that the most physical way to correct for this would be the introduction of an ion-free Stern layer, which can be achieved by ramping up the dielectric and ionic charge density functions at different density cutoffs.[70]

3.1.2. Ramping of the Dielectric Function. In most PCM models,[30,33,38] the dielectric function transition from the solute to the electrolyte is parametrized and fit (e.g., through least-squares) to reproduce neutral molecular solvation energies. However, its transferability to extended charged metal surfaces has not been investigated.

At the electrochemical interface, the metal−water interaction results in at least one ice-like bilayer of water on metal surfaces which extends 3−5 Å from the surface. This bilayer has been observed both experimentally in UHV[81] and theoretically on Pt(111).[82−84] When a potential is applied and a strong electric field is present, there is further ordering of the bilayer, which reduces the translational and rotational degrees of freedom of water.[85,86] Therefore, water near the electrochemical interface has a significantly lower dielectric constant relative to the bulk.[87−89] Such effects are not accounted for with an isotropic dielectric function that is optimized for molecular systems, even if they are charged.[90] Bonthuis and Netz evaluated the dielectric tensor at different interfaces by classical molecular dynamics simulations.[91,92] They found that constraining water close to interfaces results in a late transition of the perpendicular component of the dielectric permittivity to the bulk value at around 6−8 Å while the parallel component reaches its bulk limit within 2−4 Å. By constructing narrow channels, Fumagalli et al. measured the out-of-plane dielectric constant of water to ramp from 2 at a thickness of 10 Å up to the bulk dielectric constant of 78.4 at channel widths of over 100 nm,[93] and find that this result holds regardless of the hydrophilicity of the surface.

These findings motivate the development of more advanced PCMs for interfaces that account for the two major dielectric tensor components in order to correctly describe ice-like water layers. In terms of an isotropic dielectric function as implemented in VASPsol and other commonly used PCMs, one can in principal effectively mitigate such effects by ramping up the dielectric function over a larger distance from metal to the bulk solvent or by simply adjusting the bulk permittivity to which the dielectric function ramps. Electric double layer field effects on electrochemical reaction kinetics are commonly dominated by the vertical component of the field on the surface[12,94] which suggests that a correct description of the parallel component of the dielectric tensor might be less significant. This procedure would, however, still require a careful parametrization of the perpendicular dielectric component. Comparison of calculated reaction rates from microkinetic modeling with experimental current densities may provide one way to parametrize the appropriate dielectric ramping function, since as we will discuss later, the dielectric ramping function has a strong effect on energetics.

Figure 2 shows variation of the dielectric permittivity and *xy*-averaged ionic charge density for two values of ε_b: 78.4 (corresponding to bulk water) and 4.0 (representing constrained water) at 1.15 V vs SHE. The figure shows that this ramping of ε with the default parameters is too fast; we find that ε reaches the bulk limit within 3−4 Å of the surface, which is well within the first water bilayer. This rate of ramping is faster than the experimental[95] and theoretical investigations.[89,96]

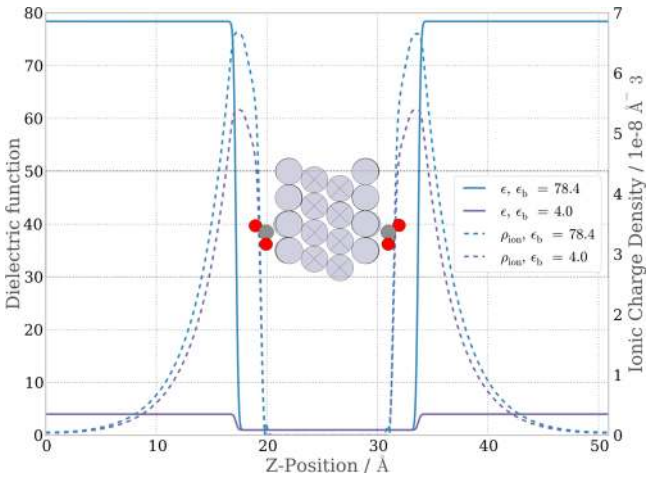

Figure 2. Increase of the *xy*-plane averaged dielectric function away from the surface for two values of ε_b, and decay of the *xy*-plane averaged ρ_{ion} for the same two bulk dielectric permittivities at a fixed potential of 1.15 V vs SHE.

We also note that here, as illustrated by Figure 1, the ionic charge is unphysically close to the metal slab and a significant proportion lies in the region of vacuum permittivity. This charge placement gives rise to a relatively constant capacitance as a function of potential in these model systems. However, it arises from charge distributed unphysically close to the

DOI: 10.1021/acscatal.8b02793
ACS Catal. 2019, 9, 920−931

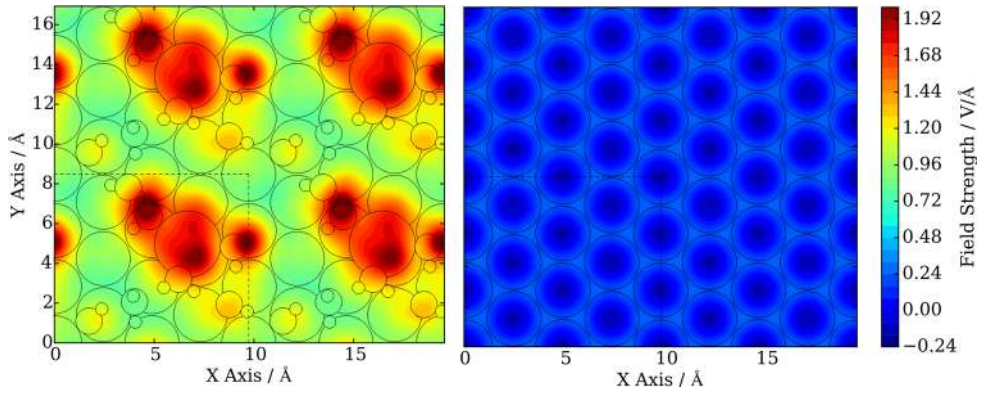

Figure 3. Left: Field distribution on Pt(111) with explicit solvent molecules and a solvated sodium ion. Right: Field distribution on Pt(111) with implicit solvation, charged to have the same work function as in the left panel. Dotted lines mark the boundaries of the unit cell.

interface where the dielectric constant ∼1, corresponding to that of vacuum.[73,97,98]

Since a decrease of the bulk permittivity would lead to an underestimation of the bulk solvent response to charged surfaces, a slow ramping of the dielectric function may be the more reliable approach. Unfortunately, however, using σ higher than the default parameter exhibits significant numerical instabilities. Further, while the ramping is indeed slower for larger σ, the onset of ramping is also moved closer to the slab, which in fact worsens the problem. These issues with σ are illustrated in SI Figure S7 and motivate the development of new dielectric function models particularly adjusted for solid−liquid interfaces.

We therefore focus our discussion on the impact of a decreased ε_b. As shown in Table 1 and SI Figure S4, the associated capacitance is lowered from 13.7 to 5.4 μF cm^{-2}. The decrease in capacitance from lowering the bulk dielectric constant synergizes with the decrease from pushing the countercharge density away from the surface; with both modifications made, the predicted capacitance drops to about 2.7 μF cm^{-2}, which is about an order of magnitude lower than experimental capacitances. We also observe that the PZC of Pt(111) varies by about 0.3 V in changing these parameters. The sensitivity of the capacitance and PZC have also been reported in ref 80 for the Li | PCM interface, and is illustrated in SI Figures S3 and S4. We note that the capacitances reported here are not unphysical, despite this model applying Gouy−Chapman theory at large concentrations (a Debye length of 3.0 Å corresponds to a bulk ion concentration of roughly 1.0 M). The primary reason for this is, as illustrated by Figure 2, the dielectric ramping region acts as an effective Stern layer, where there is charge separation across a region of relatively low dielectric constant. This can also be observed in SI Figure S8, where increasing the Debye length (which affects the double-layer capacitance but not the Helmholtz capacitance), does not significantly change the overall capacitance until the Debye length is made quite large.

3.1.3. Electric Field Distribution. The continuum description of ionic charge, using the default parameters, provides a very different field distribution from an explicit picture. Continuum models are by construction not made for reproducing properties of single electrolyte configurations but for calculating thermodynamically averaged properties. Faradaic reactions at charged electrode surfaces, however, can be driven strong local fields that do not appear in the thermodynamically averaged ion distribution.[12] The importance of ion-induced field stabilization has been investigated for several important electrochemical reactions, including the oxygen reduction reaction (ORR)[94] and CO_2 reduction.[12] The effect of including explicit ions in addition to a continuum description of the solvation and ionic charge is being studied currently, and offers one potential solution to this problem.

Figure 3 compares the field at a distance of 3 Å from the surface associated with an explicit Na^+ ion solvated by explicit waters (left) vs the LPB/PCM description at the same work function of 4.5 eV (right). This distance is associated with that of the carbon atom in CO_2 adsorbed on the surface. In the case of explicit solvent, the local field variation was calculated by the following expression:[12]

$$E_{\text{field}} = -\frac{\mathrm{d}V_{\text{diff}}}{\mathrm{d}z} \tag{9}$$

with

$$V_{\text{diff}} = V_{\text{total}} - V_{\text{electrolyte}} - V_{\text{slab}} \tag{10}$$

Here V_{total} is the ionic and Hartree potential of the total system (slab and explicit electrolyte), $V_{\text{electrolyte}}$ is the ionic and Hartree potential of the electrolyte (with no slab), and V_{slab} is the ionic and Hartree potential of the slab (with no electrolyte).

In the case of implicit solvation, the field is calculated by eq 9, but with V_{diff} calculated instead as

$$V_{\text{diff}} = V_{\text{charged}} - V_{\text{uncharged}} \tag{11}$$

Here, V_{charged} refers to the potential of the charged surface, including the potential due to counterions, of the Pt(111) surface, and $V_{\text{uncharged}}$ refers to the potential of the uncharged (but solvated) Pt(111) surface. Because the ions are placed very close to the surface, this field increases rapidly and then quickly decays to 0 about 1 Å from the surface. For sampling the field strength, we choose the z position to be between carbon and oxygen on adsorbed CO_2.

As can be seen, there are stark differences in the field distributions in the two models. A LPB/PCM model obviously cannot capture the variation of the electric field in the *xy* plane associated with an explicit cation and the associated effects on the energetics of reaction intermediates. The LPB/PCM field is also significantly smaller, which arises from the placement of continuum charge extremely close to the surface (Figure 2) and the corresponding fast decay of the field along *z*. This could lead to an underestimation of local field effects on reaction kinetics.

DOI: 10.1021/acscatal.8b02793
ACS Catal. 2019, 9, 920−931

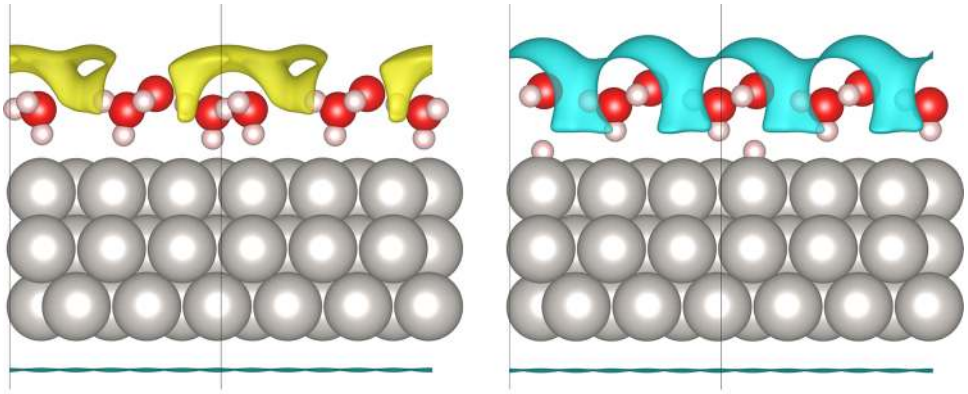

Figure 4. Ionic countercharge density isosurface plot illustrating the charge intercalation into the explicit water layer for the (a) initial (charged) state, and (b) final (uncharged) state. Here the isosurface density value is 1.4×10^{-4} eÅ^{-3}, with yellow representing positive electron density, and blue representing negative electron density. Both the initial and final state are charged to a potential of 0.0 V vs SHE.

3.1.4. Effects of Explicit Water. Recent simulations have made use of a hybrid approach which includes a few explicit waters at the metal | PCM interface. These approaches would allow for the explicit solvation of the ions that participate in charge transfer reactions,[43,99] and for a more physical description of charge and dielectric constant at the interface. Here we consider the Volmer reaction to be a proton−electron transfer to the surface, with the initial state being the proton in the inner Helmholtz plane, shown in Figure 4. SI Figure S9 shows the corresponding q vs U curves for the initial and final states. We use a static water structure, corresponding to the hexagonal structure observed by Ogasawara and co-workers.[81]

Overall, the introduction of the explicit solvent layer leads to significant deviations in capacitance from experimental values of ∼20 μF cm^{-2}.[100] Because of the larger average ion-metal distances introduced by the explicit water (illustrated by the charge density isosurfaces of Figure 4), the capacitances are lowered. At the default ϵ_b of 78, the capacitance is 9.2 μF cm^{-2} in the charged (initial) state, and 9.9 μF cm^{-2} in the uncharged (final) state; and at a bulk dielectric constant of 4 it is further decreased 5.1 μF cm^{-2} in the initial state, and 5.2 μF cm^{-2} in the final state. The work published in ref 101 also finds a decreased capacitance when an explicit solvent layer is added to the simulation. They find that the capacitance increases further, to 27 μF cm^{-2} with an additional bilayer of explicit solvent. However, we find this actually decreases the capacitance, to about 6.3 μF cm^{-2}, shown in SI Figure S10.

We note also that, under default model parameters, the continuum charge unphysically enters the spaces within the explicit hexagonal water structure, as illustrated in Figure 4. This mixture of implicit and explicit models within the Helmholtz plane may also yield unintended effects on reaction energetics of interest.

Overall, careful parametrization, and perhaps a modification to the model to prevent ion intercalation into the explicit region, would therefore be necessary in order to obtain a more physical model and to obtain agreement with experimental capacitances.

3.2. Constant Potential Simulations. A major challenge associated with ab initio simulations of electrochemical activation energies in fully explicit model systems is that the simulations operate at a constant number of electrons, while physical systems operate at constant potential. This issue can be mitigated in large cell calculations that mimic the physical system[102] or in extrapolation schemes to the large cell limit based on simple capacitor models of the interface, illustrated in SI Figure S11.[20,58]

PB continuum models provide a way to keep the potential constant by varying the surface and electrolyte charge density. This allows to compensate for the continuous shifts in interface dipoles being associated with work function shifts during an electrochemical reaction process. In such calculations, intermediate images between the initial and final state are created, and a transition state search is performed using methods such as the dimer method[103] and the nudged elastic band (NEB).[104,105] The electronic and continuum ionic charge of the images are varied such that the entire reaction pathway is fixed at a given potential. This approach has been applied in a number of recent mechanistic studies.[42,43,99,106,107]

3.2.1. Kinetics and Timescales. A fundamental challenge with the physical picture of LPB/PCM schemes for electrochemical activation barriers at constant potential is the assumption that ions follow adiabatically the atomic motion associated with the electrochemical reactions. However, the atomic motion associated with reaction events occurs on much faster timescales than solvent reorganization and ionic diffusion. The physical movement of atoms during a proton transfer is on the order of femtoseconds, while ion rearrangement occurs on the order of pico- to nanoseconds.[108] Indeed, the classical theories of electron transfer such as outer-sphere Marcus theory predict that electron transfer proceeds diabatically, with no solvent reorganization.[109,110] This was more recently extended to proton transfer theory, where rate constants for a wide variety of PCET reactions were predicted with good agreement to experimental measurements.[111]

We estimate the timescales for ion rearrangement as follows. Table 2 shows the experimentally determined[112] ion mobilities

Table 2. Experimentally Determined[112,117] Ion Mobilities for Common Ions at 298 K

ion	mobility/10^{-8} m^2 V^{-1} s^{-1}	D/10^{-9} m^2 s^{-1}	time/ps
Na^+	5.19	1.34	17
K^+	7.62	1.97	11
Cl^-	7.91	2.05	11
OH^-	20.64	5.34	4
H^+	36.23	9.37	2

DOI: 10.1021/acscatal.8b02793
ACS Catal. 2019, 9, 920−931

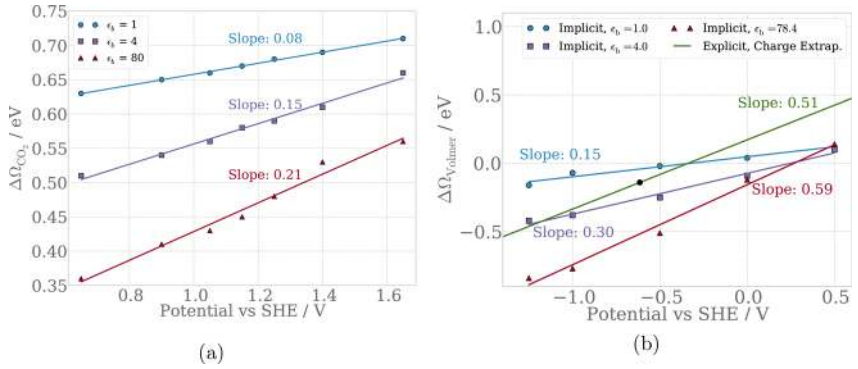

Figure 5. Potential dependence of (a) CO_2 adsorption and (b) Volmer reaction on Pt(111) at varying bulk solvent dielectric constant ϵ_b, compared to an explicitly calculated ΔG via charge extrapolation.[20,58]

in aqueous media. To convert these mobilities into a diffusion constant, we use the Einstein relation[113]

$$D = \frac{\mu_q k_B T}{q} \tag{12}$$

where μ_q is the electrical ion mobility, k_B the Boltzmann constant and q the charge of the ion. From D, one can arrive at a characteristic time for the ion to diffuse over a length scale with the following expression:[114]

$$t = \frac{L^2}{4D} \tag{13}$$

Here t is the characteristic diffusion time, L is a length scale.

Assuming the Debye length of 3 Å as a lower bound estimate of the length scale for the double layer response to charging the surface, we obtain an estimated time of 17 ps for Na^+ rearrangement using eq 13. The estimates for various other ions are shown in Table 2, and they all fall within the same order of magnitude. Previous work using Brownian dynamics simulations has also shown that it takes on the order of 1 ns for the electrochemical double layer to relax.[115] All these timescale estimates together suggest that the relaxation of the double layer is significantly slower than the femtosecond timescale of atomic motion during a reaction event. The timescales of reaction rates are also significantly longer than that for a given reaction event. On Pt in acidic solutions, the timescale of the hydrogen evolution, obtained from Arrhenius plots, is between 5 and 200 ps at low overpotentials (below 60 mV).[116] Reaction events are therefore exceedingly rare, and this element is captured through large cell calculations or through the extrapolation schemes discussed above.[58] Ionic motion should hence not be assumed to follow adiabatically the motion associated with reaction events.

3.2.2. Energetics and Field Variations. In addition to the fundamental challenge of timescales, we discuss two further technical challenges associated with PCMs of reaction activation energies. First, the energetics, like the interfacial capacitance and PZC, are sensitive to parametrization, and uncertainties in the parametrization translates to uncertainties in the energetics. As discussed above, a lowered ϵ_b from the bulk value of 78 and an increased $\tilde{\rho}_{el,cut}$ from the default value would give a more realistic description of the dielectric constant and the position of ions in the interface region, respectively. The effect of the dielectric constant (ϵ_b = 78.4, 4.0, and 1.0) on the (a) CO_2 adsorption energy and (b) Volmer reaction energy as a function of potential are shown in Figure 5. The Volmer reaction Gibbs free energy using a fully explicit approach, with extrapolation to the constant potential limit,[20,58] is also shown for comparison, and deviates from the implicit values, which can be attributed to the number of challenges discussed above.

Finally, while continuous charging of the interface allows for the calculation of reaction energetics at a constant potential, the corresponding surface charge density and electric field varies along the reaction path due to the charging response to the shift in interface dipole. Figure S9 (a) in the SI shows that the q at a fixed potential varies by about 0.4 electrons between IS and FS for CO_2 adsorption in a 4 × 4 supercell, and by 0.6 electrons between the IS and FS the Volmer reaction in a 4 × 3 supercell. In the limit where q is distributed uniformly, e.g. in a parallel plate capacitor, these shifts correspond to a shift in E_{field} of 1.2 V $Å^{-1}$ and 1.3 V $Å^{-1}$ for CO_2 adsorption and Volmer, respectively. These variations in field would impact the energetics of polar adsorbates, or explicit waters applied in hybrid explicit-implicit models, and likely contribute to the difference observed between the infinite cell limit (extrapolated) and LPB-PCM calculations observed in Figure 5b. It may be possible to correct for these effects; this is the focus of future work.

4. CONCLUSIONS AND OUTLOOK

Modern electronic structure theory consists of a hierarchy of approximate computational models that introduce trade offs between accuracy and computational feasibility, as exemplified by the five rungs on Perdew's Jacob's ladder classification.[118] The challenge of modeling the solid−liquid electrode−electrolyte interface in electrocatalysis invites the development of a similar range of models. The formally exact treatment, fully molecular, and grand-canonical in both electrons and electrolyte ions, is a challenge that lies beyond present-day computing resources if one is to obtain converged statistical sampling. There is therefore a computational necessity to also consider simpler models in order to model electrocatalysis today. One might roughly group such models into four groups: (1) Bias-free and electrolyte free modeling, as exemplified by early studies using the computational hydrogen electrode (CHE).[56,119−123] This approach captures the leading thermodynamic effects of applied bias, but neglects all bias and electrolyte induced changes in the electronic structure. (2) Bias-free, fully explicit solvation models, illustrated by many thermodynamic studies of electrochemical reactions using the CHE.[12,17,102,124,125] (3) Fully explicit solvent models, which rely on the CHE and extrapolation methods to obtain

DOI: 10.1021/acscatal.8b02793
ACS Catal. 2019, 9, 920−931

potential-dependent reaction energetics. Because of constraints in computing time, rigorous statistical sampling is a challenge.[16,20,57,58,126] (4) Fully implicit electrolyte with applied bias, treated by linearized Poisson−Boltzmann/polarizable continuum models (LPB-PCM).[30,32,34,37,40,42,43,71,74] This mixed atomistic-continuum approach captures changes in electronic structure of surface species and interactions with the charged electrode to permit bias-dependent calculations, but neglects specific molecular solvent and electrolyte ion effects. We have carefully examined the challenges of the LPB-PCM in this Perspective.

LPB-PCMs provide a computationally inexpensive way to model the electrochemical interface, but come with a number of open challenges. Since ions are assumed to have no finite size, the ionic charge density is placed too close to the surface, Additionally, the dielectric constant increases to the bulk limit too quickly. These issues can be mitigated by modifying the charge density cutoff $\tilde{\rho}_{\mathrm{el,cut}}$ or the bulk dielectric constant, respectively. Both of these adjustments, while improving the solvent physics, render the LPB/PCM unable to reproduce experimental capacitances. LPB/PCM also necessarily smears out the ion density across the entire electrolyte and therefore gives essentially uniform fields, which may not capture the effect of localized field variations associated with explicit cations on reaction energetics. Further, the inclusion of a layer of explicit solvent, which can provide a more realistic solvation of the ions at the interface, can at the same time lead to unphysical placement of ionic countercharge and deviations of the interfacial capacitance from experimental values.

The determination of electrochemical reaction energetics using LPB/PCM also poses several challenges. LPB/PCM schemes allow for constant potential calculations through continuous variations in surface charge along with interface dipole shifts. The primary challenge with such an approach is the assumption that the double layer charging response follows adiabatically the atomic motion of reaction events, even though the former occurs at a significantly slower timescale. We also find reaction energetics to be sensitive to parametrization such that uncertainties in the parameters translate to uncertainties in energetics. Finally, while the charging of the interface gives rise to constant potential conditions, it also gives rise to variations in electric fields along the reaction pathway.

A modified Poisson−Boltzmann approach to modeling the electrochemical reaction energetics would mitigate some of the aforementioned issues, but not all. In particular, the countercharge placement and dielectric function behavior could be mitigated by the inclusion of a Stern layer, as has been implemented[30,70] for the FHI-aims code. However, this modification would not solve the localization of the field due to ions, and furthermore all continuum models will face challenges in the calculation of electrochemical barriers. The continuum model may still be useful in evaluating the charging response of systems of interest or find practical application in the problem of band misalignment of water[24] found in explicit solvent electrochemical barrier calculations. It is also quite possible that a hybrid approach, where solvent molecules are modeled by a continuum, but the work function is modified by explicitly solvated ions, could be used. This would mitigate the need to determine thermodynamically averaged water structures at the interface. This approach would also avoid the problems associated with the classical treatment of the countercharge and the intrinsic locality of the field, but retain the ability of the continuum model to handle solvation energies.

■ ASSOCIATED CONTENT

Supporting Information

The Supporting Information is available free of charge on the ACS Publications website at DOI: 10.1021/acscatal.8b02793.

Figures and tables referenced in the text; tables of all data required to reproduce the figures in this work (PDF)

■ AUTHOR INFORMATION

Corresponding Author

*E-mail: kchan@fysik.dtu.dk.

ORCID

Joseph A. Gauthier: 0000-0001-9542-0988
Colin F. Dickens: 0000-0002-6151-0755
Alexis T. Bell: 0000-0002-5738-4645
Martin Head-Gordon: 0000-0002-4309-6669
Karen Chan: 0000-0002-6897-1108

Notes

The authors declare no competing financial interest.

■ ACKNOWLEDGMENTS

We would like to thank Dr. Dan Wang and Prof. Ravishankar Sundararaman for their insightful discussions. Support from the U.S. Department of Energy, Office of Basic Energy Science, Chemical Sciences, Geosciences, and Biosciences Division, to the SUNCAT Center for Interface Science and Catalysis is gratefully acknowledged. A.J.G was supported by the Joint Center for Artificial Photosynthesis, a DOE Energy Innovation Hub, supported through the Office of Science of the U.S. Department of Energy under Award DE-SC00004993. A.T.B. and M.H-G acknowledge support from the U.S. Department of Energy, Office of Science, Office of Advanced Scientific Computing Research, Scientific Discovery through Advanced Computing (SciDAC) program. C.F.D. acknowledges fellowship support from the National Science Foundation Graduate Research Fellowship (Grant No. DGE-114747). Some of the computing for this project was performed on the Sherlock cluster. We would like to thank Stanford University and the Stanford Research Computing Center for providing computational resources and support that contributed to these research results. This research used resources of the National Energy Research Scientific Computing Center (NERSC), a U.S. Department of Energy Office of Science User Facility operated under Contract No. DE-AC02-05CH11231.

■ REFERENCES

(1) Helmholtz, H. Ueber Einige Gesetze der Vertheilung elektrischer Ströme in körperlichen Leitern mit Anwendung auf die Thierisch-Elektrischen Versuche. *Ann. Phys.* **1853**, *165*, 211−233.

(2) Gouy, M. Sur la Constitution de la Charge Électrique à la Surface d'un Électrolyte. *J. Phys. Theor. Appl.* **1910**, *9*, 457−468.

(3) Chapman, D. L. A Contribution to the Theory of Electrocapillarity. *Philos. Mag.* **1913**, *25*, 475−481.

(4) Stern, O. Zur Theorie der Elektrolytischen Doppelschicht. *Zeitschrift für Elektrochemie* **1924**, *30*, 508−516.

(5) Bockris, J. OM.; Devanathan, M. A. V.; Muller, K. On the Structure of Charged Interfaces. *Proc. R. Soc. London, Ser. A* **1963**, *274*, 55.

DOI: 10.1021/acscatal.8b02793
ACS Catal. 2019, 9, 920−931

(6) Grahame, D. C. The Electrical Double Layer and the Theory of Electrocapillarity. *Chem. Rev.* **1947**, *41*, 441−501.
(7) Cheng, T.; Xiao, H.; Goddard, W. A., III Free-Energy Barriers and Reaction Mechanisms for the Electrochemical Reduction of CO on the Cu (100) Surface, Including Multiple Layers of Explicit Solvent at pH 0. *J. Phys. Chem. Lett.* **2015**, *6*, 4767−4773.
(8) Cheng, T.; Xiao, H.; Goddard, W. A. Full Atomistic Reaction Mechanism With Kinetics for CO Reduction on Cu(100) from Ab Initio Molecular Dynamics Free-Energy Calculations at 298 K. *Proc. Natl. Acad. Sci. U. S. A.* **2017**, *114*, 1795−1800.
(9) Sakong, S.; Groß, A. The Importance of the Electrochemical Environment in the Electro-Oxidation of Methanol on Pt(111). *ACS Catal.* **2016**, *6*, 5575−5586.
(10) Sakong, S.; Naderian, M.; Mathew, K.; Hennig, R. G.; Groß, A. Density Functional Theory Study of the Electrochemical Interface Between a Pt Electrode and an Aqueous Electrolyte Using an Implicit Solvent Method. *J. Chem. Phys.* **2015**, *142*, 234107.
(11) Neurock, M.; Janik, M.; Wieckowski, A. A First Principles Comparison of the Mechanism and Site Requirements for the Electrocatalytic Oxidation of Methanol and Formic Acid Over Pt. *Faraday Discuss.* **2009**, *140*, 363−378.
(12) Chen, L. D.; Urushihara, M.; Chan, K.; Nørskov, J. K. Electric Field Effects in Electrochemical CO2 Reduction. *ACS Catal.* **2016**, *6*, 7133−7139.
(13) Sandberg, R. B.; Montoya, J. H.; Chan, K.; Nørskov, J. K. CO-CO Coupling on Cu Facets: Coverage, Strain and Field Effects. *Surf. Sci.* **2016**, *654*, 56−62.
(14) Liu, X.; Xiao, J.; Peng, H.; Hong, X.; Chan, K.; Nørskov, J. K. Understanding Trends in Electrochemical Carbon Dioxide Reduction Rates. *Nat. Commun.* **2017**, *8*, 15438.
(15) Saleheen, M.; Heyden, A. Liquid Phase Modeling in Heterogeneous Catalysis. *ACS Catal.* **2018**, *8*, 2188−2194.
(16) Tripković, V.; Skúlason, E.; Siahrostami, S.; Nørskov, J. K.; Rossmeisl, J. The Oxygen Reduction Reaction Mechanism on Pt (111) From Density Functional Theory Calculations. *Electrochim. Acta* **2010**, *55*, 7975−7981.
(17) Gauthier, J.; Dickens, C. F.; Chen, L. D.; Doyle, A. D.; Norskov, J. K. Solvation Effects for Oxygen Evolution Reaction Catalysis on IrO_2 (110). *J. Phys. Chem. C* **2017**, *121*, 11455.
(18) Nie, X.; Luo, W.; Janik, M. J.; Asthagiri, A. Reaction Mechanisms of CO2 Electrochemical Reduction on Cu (111) Determined With Density Functional Theory. *J. Catal.* **2014**, *312*, 108−122.
(19) Janik, M. J.; Taylor, C. D.; Neurock, M. First Principles Analysis of the Electrocatalytic Oxidation of Methanol and Carbon Monoxide. *Top. Catal.* **2007**, *46*, 306−319.
(20) Chan, K.; Nørskov, J. K. Potential Dependence of Electrochemical Barriers From Ab Initio Calculations. *J. Phys. Chem. Lett.* **2016**, *7*, 1686−1690.
(21) Kristoffersen, H. H.; Vegge, T.; Hansen, H. A. OH formation and H_2 Adsorption at the Liquid Water-Pt (111) Interface. *Chemical Science* **2018**, *9*, 6912−6921.
(22) Sakong, S.; Groß, A. Methanol Oxidation on Pt(111) from First-Principles in Heterogeneous and Electrocatalysis. *Electrocatalysis* **2017**, *8*, 577.
(23) Bonnet, N.; Morishita, T.; Sugino, O.; Otani, M. First-Principles Molecular Dynamics at a Constant Electrode Potential. *Phys. Rev. Lett.* **2012**, *109*, 266101.
(24) Björketun, M. E.; Zeng, Z.; Ahmed, R.; Tripkovic, V.; Thygesen, K. S.; Rossmeisl, J. Avoiding Pitfalls in the Modeling of Electrochemical Interfaces. *Chem. Phys. Lett.* **2013**, *555*, 145−148.
(25) Lozovoi, A.; Alavi, A.; Kohanoff, J.; Lynden-Bell, R. Ab Initio Simulation of Charged Slabs at Constant Chemical Potential. *J. Chem. Phys.* **2001**, *115*, 1661−1669.
(26) Taylor, C. D.; Wasileski, S. A.; Filhol, J.-S.; Neurock, M. First Principles Reaction Modeling of the Electrochemical Interface: Consideration and Calculation of a Tunable Surface Potential From Atomic and Electronic Structure. *Phys. Rev. B: Condens. Matter Mater. Phys.* **2006**, *73*, 165402.
(27) Mamatkulov, M.; Filhol, J.-S. An Ab Initio Study of Electrochemical vs. Electromechanical Properties: The Case of CO Adsorbed on a Pt(111) Surface. *Phys. Chem. Chem. Phys.* **2011**, *13*, 7675−7684.
(28) Fang, Y.-H.; Liu, Z.-P. Surface Phase Diagram and Oxygen Coupling Kinetics on Flat and Stepped Pt Surfaces Under Electrochemical Potentials. *J. Phys. Chem. C* **2009**, *113*, 9765−9772.
(29) Fang, Y.-H.; Liu, Z.-P. Mechanism and Tafel Lines of Electro-Oxidation of Water to Oxygen on RuO_2 (110). *J. Am. Chem. Soc.* **2010**, *132*, 18214−18222.
(30) Ringe, S.; Oberhofer, H.; Hille, C.; Matera, S.; Reuter, K. Function-Space-Based Solution Scheme for the Size-Modified Poisson-Boltzmann Equation in Full-Potential DFT. *J. Chem. Theory Comput.* **2016**, *12*, 4052−4066.
(31) Jinnouchi, R.; Anderson, A. B. Aqueous and Surface Redox Potentials From Self-Consistently Determined Gibbs Energies. *J. Phys. Chem. C* **2008**, *112*, 8747−8750.
(32) Mathew, K.; Hennig, R. G. Implicit Self-Consistent Description of Electrolyte in Plane-Wave Density-Functional Theory. 2016, *arXiv:1601.03346*. arXiv e-Print archive. https://arxiv.org/abs/1601.03346.
(33) Fisicaro, G.; Genovese, L.; Andreussi, O.; Marzari, N.; Goedecker, S. A generalized Poisson and Poisson-Boltzmann solver for electrostatic environments. *J. Chem. Phys.* **2016**, *144*, 014103.
(34) Fang, Y.-H.; Wei, G.-F.; Liu, Z.-P. Theoretical Modeling of Electrode/Electrolyte Interface From First-Principles Periodic Continuum Solvation Method. *Catal. Today* **2013**, *202*, 98−104.
(35) Letchworth-Weaver, K.; Arias, T. Joint Density Functional Theory of the Electrode-Electrolyte Interface: Application to Fixed Electrode Potentials, Interfacial Capacitances, and Potentials of Zero Charge. *Phys. Rev. B: Condens. Matter Mater. Phys.* **2012**, *86*, 075140.
(36) Keilbart, N.; Okada, Y.; Feehan, A.; Higai, S.; Dabo, I. Quantum-Continuum Simulation of the Electrochemical Response of Pseudocapacitor Electrodes Under Realistic Conditions. *Phys. Rev. B: Condens. Matter Mater. Phys.* **2017**, *95*, 115423.
(37) Sundararaman, R.; Schwarz, K. Evaluating Continuum Solvation Models for the Electrode-Electrolyte Interface: Challenges and Strategies for Improvement. *J. Chem. Phys.* **2017**, *146*, 084111.
(38) Minezawa, N.; Kato, S. Efficient Implementation of Three-Dimensional Reference Interaction Site Model Self-Consistent-Field Method: Application to Solvatochromic Shift Calculations. *J. Chem. Phys.* **2007**, *126*, 054511.
(39) Mathew, K.; Sundararaman, R.; Letchworth-Weaver, K.; Arias, T.; Hennig, R. G. Implicit Solvation Model for Density-Functional Study of Nanocrystal Surfaces and Reaction Pathways. *J. Chem. Phys.* **2014**, *140*, 084106.
(40) Andreussi, O.; Dabo, I.; Marzari, N. Revised Self-Consistent Continuum Solvation in Electronic-Structure Calculations. *J. Chem. Phys.* **2012**, *136*, 064102.
(41) Sundararaman, R.; Goddard, W. A., III The Charge-Asymmetric Nonlocally Determined Local-Electric (CANDLE) Solvation Model. *J. Chem. Phys.* **2015**, *142*, 064107.
(42) Ping, Y.; Nielsen, R. J.; Goddard, W. A. The Reaction Mechanism with Free Energy Barriers at Constant Potentials for the Oxygen Evolution Reaction at the IrO2 (110) Surface. *J. Am. Chem. Soc.* **2017**, *139*, 149−155.
(43) Goodpaster, J. D.; Bell, A. T.; Head-Gordon, M. Identification of Possible Pathways for C-C Bond Formation During Electrochemical Reduction of CO2: New Theoretical Insights From an Improved Electrochemical Model. *J. Phys. Chem. Lett.* **2016**, *7*, 1471−1477.
(44) Steinmann, S. N.; Sautet, P. Assessing a First-Principles Model of an Electrochemical Interface by Comparison with Experiment. *J. Phys. Chem. C* **2016**, *120*, 5619−5623.
(45) Sundararaman, R.; Letchworth-Weaver, K.; Schwarz, K. A.; Gunceler, D.; Ozhabes, Y.; Arias, T. JDFTx: Software for Joint Density-Functional Theory. *SoftwareX* **2017**, *6*, 278−284.

DOI: 10.1021/acscatal.8b02793
ACS Catal. 2019, 9, 920−931

(46) Sundararaman, R.; Goddard, W. A., III; Arias, T. A. Grand Canonical Electronic Density-Functional Theory: Algorithms and Applications to Electrochemistry. *J. Chem. Phys.* **2017**, *146*, 114104.
(47) Xiao, H.; Cheng, T.; Goddard, W. A., III; Sundararaman, R. Mechanistic Explanation of the pH Dependence and Onset Potentials for Hydrocarbon Products From Electrochemical Reduction of CO on Cu (111). *J. Am. Chem. Soc.* **2016**, *138*, 483−486.
(48) Otani, M.; Sugino, O. First-Principles Calculations of Charged Surfaces and Interfaces: A Plane-Wave Nonrepeated Slab Approach. *Phys. Rev. B: Condens. Matter Mater. Phys.* **2006**, *73*, 115407.
(49) Hamada, I.; Sugino, O.; Bonnet, N.; Otani, M. Improved Modeling of Electrified Interfaces Using the Effective Screening Medium Method. *Phys. Rev. B: Condens. Matter Mater. Phys.* **2013**, *88*, 155427.
(50) Hamada, I.; Otani, M.; Sugino, O.; Morikawa, Y. Green's Function Method for Elimination of the Spurious Multipole Interaction in the Surface/Interface Slab Model. *Phys. Rev. B: Condens. Matter Mater. Phys.* **2009**, *80*, 165411.
(51) Kovalenko, A.; Hirata, F. Self-Consistent Description of a Metal-water Interface by the Kohn-Sham Density Functional Theory and the Three-Dimensional Reference Interaction Site Model. *J. Chem. Phys.* **1999**, *110*, 10095−10112.
(52) Kovalenko, A. *Molecular Theory of Solvation*; Springer: Netherlands, 2004; pp 169−275.
(53) Nishihara, S.; Otani, M. Hybrid Solvation Models for Bulk, Interface, and Membrane: Reference Interaction Site Methods Coupled With Density Functional Theory. *Phys. Rev. B: Condens. Matter Mater. Phys.* **2017**, *96*, 115429.
(54) Sha, Y.; Yu, T. H.; Liu, Y.; Merinov, B. V.; Goddard, W. A., III Theoretical Study of Solvent Effects on the Platinum-Catalyzed Oxygen Reduction Reaction. *J. Phys. Chem. Lett.* **2010**, *1*, 856−861.
(55) Jinnouchi, R.; Anderson, A. B. Electronic Structure Calculations of Liquid-Solid Interfaces: Combination of Density Functional Theory and Modified Poisson-Boltzmann Theory. *Phys. Rev. B: Condens. Matter Mater. Phys.* **2008**, *77*, 245417.
(56) Nørskov, J. K.; Rossmeisl, J.; Logadottir, A.; Lindqvist, L.; Kitchin, J. R.; Bligaard, T.; Jonsson, H. Origin of the Overpotential for Oxygen Reduction at a Fuel-Cell Cathode. *J. Phys. Chem. B* **2004**, *108*, 17886−17892.
(57) Montoya, J. H.; Shi, C.; Chan, K.; Nørskov, J. K. Theoretical Insights Into a CO Dimerization Mechanism in CO2 Electroreduction. *J. Phys. Chem. Lett.* **2015**, *6*, 2032−2037.
(58) Chan, K.; Nørskov, J. K. Electrochemical barriers Made Simple. *J. Phys. Chem. Lett.* **2015**, *6*, 2663−2668.
(59) Kresse, G.; Hafner, J. Ab Initio Molecular Dynamics for Liquid Metals. *Phys. Rev. B: Condens. Matter Mater. Phys.* **1993**, *47*, 558−561.
(60) Kresse, G.; Furthmüller, J. Efficient Iterative Schemes for Ab Initio Total-Energy Calculations Using a Plane-Wave Basis Set. *Phys. Rev. B: Condens. Matter Mater. Phys.* **1996**, *54*, 11169−11186.
(61) Kresse, G.; Furthmüller, J. Efficiency of Ab-Initio Total Energy Calculations for Metals and Semiconductors Using a Plane-Wave Basis Set. *Comput. Mater. Sci.* **1996**, *6*, 15−50.
(62) Kresse, G.; Joubert, D. From Ultrasoft Pseudopotentials to the Projector Augmented-Wave Method. *Phys. Rev. B: Condens. Matter Mater. Phys.* **1999**, *59*, 1758−1775.
(63) Monkhorst, H. J.; Pack, J. D. Special Points for Brillouin-Zone Integrations. *Phys. Rev. B* **1976**, *13*, 5188.
(64) Hammer, B.; Hansen, L. B.; Nørskov, J. K. Improved Adsorption Energetics Within Density-Functional Theory Using Revised Perdew-Burke-Ernzerhof Functionals. *Phys. Rev. B: Condens. Matter Mater. Phys.* **1999**, *59*, 7413.
(65) Perdew, J. P.; Burke, K.; Ernzerhof, M. Generalized Gradient Approximation Made Simple. *Phys. Rev. Lett.* **1996**, *77*, 3865−3868.
(66) Wellendorff, J.; Silbaugh, T. L.; Garcia-Pintos, D.; Nørskov, J. K.; Bligaard, T.; Studt, F.; Campbell, C. T. A Benchmark Database for Adsorption Bond Energies to Transition Metal Surfaces and Comparison to Selected DFT Functionals. *Surf. Sci.* **2015**, *640*, 36−44.
(67) Tonigold, K.; Groß, A. Dispersive Interactions in Water Bilayers at Metallic Surfaces: A Comparison of the PBE and RPBE Functional Including Semiempirical Dispersion Corrections. *J. Comput. Chem.* **2012**, *33*, 695−701.
(68) Bengtsson, L. Dipole Correction for Surface Supercell Calculations. *Phys. Rev. B: Condens. Matter Mater. Phys.* **1999**, *59*, 12301.
(69) Scherlis, D. A.; Fattebert, J.-L.; Gygi, F.; Cococcioni, M.; Marzari, N. A Unified Electrostatic and Cavitation Model for First-Principles Molecular Dynamics in Solution. *J. Chem. Phys.* **2006**, *124*, 074103.
(70) Ringe, S.; Oberhofer, H.; Reuter, K. Transferable Ionic Parameters for First-Principles Poisson-Boltzmann Solvation Calculations: Neutral Solutes in Aqueous Monovalent Salt Solutions. *J. Chem. Phys.* **2017**, *146*, 134103.
(71) Steinmann, S. N.; Sautet, P.; Michel, C. Solvation Free Energies for Periodic Surfaces: Comparison of Implicit and Explicit Solvation Models. *Phys. Chem. Chem. Phys.* **2016**, *18*, 31850−31861.
(72) Fisicaro, G.; Genovese, L.; Andreussi, O.; Mandal, S.; Nair, N. N.; Marzari, N.; Goedecker, S. Soft-Sphere Continuum Solvation in Electronic-Structure Calculations. *J. Chem. Theory Comput.* **2017**, *13*, 3829−3845.
(73) Schmickler, W.; Santos, E. *Interfacial Electrochemistry*; Springer Science & Business Media: New York, 2010.
(74) Steinmann, S. N.; Michel, C.; Schwiedernoch, R.; Sautet, P. Impacts of Electrode Potentials and Solvents on the Electroreduction of CO_2: A Comparison of Theoretical Approaches. *Phys. Chem. Chem. Phys.* **2015**, *17*, 13949−13963.
(75) Trasatti, S.; Lust, E. *Modern Aspects of Electrochemistry*; Springer, 2002; pp 1−215.
(76) Hamm, U.; Kramer, D.; Zhai, R.; Kolb, D. The PZC of Au (111) and Pt (111) in a Perchloric Acid Solution: An Ex Situ Approach to the Immersion Technique. *J. Electroanal. Chem.* **1996**, *414*, 85−89.
(77) Trasatti, S. The Absolute Electrode Potential: An Explanatory Note. *Pure Appl. Chem.* **1986**, *58*, 955−966.
(78) Resasco, J.; Chen, L. D.; Clark, E.; Tsai, C.; Hahn, C.; Jaramillo, T. F.; Chan, K.; Bell, A. T. Promoter Effects of Alkali Metal Cations During Electrocatalytic Carbon Dioxide Reduction. *J. Am. Chem. Soc.* **2017**, *139*, 11277.
(79) Pajkossy, T.; Kolb, D. M. Double Layer Capacitance of Pt (111) Single Crystal Electrodes. *Electrochim. Acta* **2001**, *46*, 3063−3071.
(80) Lespes, N.; Filhol, J. S. Using Implicit Solvent in Ab Initio Electrochemical Modeling: Investigating Li+/Li Electrochemistry at a Li/Solvent Interface. *J. Chem. Theory Comput.* **2015**, *11*, 3375−3382.
(81) Ogasawara, H.; Brena, B.; Nordlund, D.; Nyberg, M.; Pelmenschikov, A.; Pettersson, L.; Nilsson, A. Structure and Bonding of Water on Pt (111). *Phys. Rev. Lett.* **2002**, *89*, 276102.
(82) Groß, A.; Gossenberger, F.; Lin, X.; Naderian, M.; Sakong, S.; Roman, T. Water Structures at Metal Electrodes Studied by Ab Initio Molecular Dynamics Simulations. *J. Electrochem. Soc.* **2014**, *161*, E3015−E3020.
(83) Roman, T.; Groß, A. Structure of Water Layers on Hydrogen-Covered Pt Electrodes. *Catal. Today* **2013**, *202*, 183−190.
(84) Liu, Y.; Kawaguchi, T.; Pierce, M.; Komanicky, V.; You, H. Layering and Ordering in Electrochemical Double Layers. *J. Phys. Chem. Lett.* **2018**, *9*, 1265.
(85) Vegiri, A. Dynamic Response of Liquid Water to an External Static Electric Field At T= 250 K. *J. Mol. Liq.* **2004**, *112*, 107−116.
(86) Druchok, M.; Holovko, M. Structural Changes in Water Exposed to Electric Fields: A Molecular Dynamics Study. *J. Mol. Liq.* **2015**, *212*, 969−975.
(87) Dinpajooh, M.; Matyushov, D. V. Dielectric Constant of Water in the Interface. *J. Chem. Phys.* **2016**, *145*, 014504.
(88) Yeh, I.-C.; Berkowitz, M. L. Dielectric Constant of Water at High Electric Fields: Molecular Dynamics Study. *J. Chem. Phys.* **1999**, *110*, 7935−7942.

DOI: 10.1021/acscatal.8b02793
ACS Catal. 2019, 9, 920−931

(89) Senapati, S.; Chandra, A. Dielectric Constant of Water Confined in a Nanocavity. *J. Phys. Chem. B* **2001**, *105*, 5106−5109.
(90) Dupont, C.; Andreussi, O.; Marzari, N. Self-Consistent Continuum Solvation (SCCS): The Case of Charged Systems. *J. Chem. Phys.* **2013**, *139*, 214110.
(91) Bonthuis, D. J.; Netz, R. R. Beyond the Continuum: How Molecular Solvent Structure Affects Electrostatics and Hydrodynamics at Solid-Electrolyte Interfaces. *J. Phys. Chem. B* **2013**, *117*, 11397−11413.
(92) Bonthuis, D. J.; Netz, R. R. Unraveling the Combined Effects of Dielectric and Viscosity Profiles on Surface Capacitance, Electro-Osmotic Mobility, and Electric Surface Conductivity. *Langmuir* **2012**, *28*, 16049−16059.
(93) Fumagalli, L.; Esfandiar, A.; Fabregas, R.; Hu, S.; Ares, P.; Janardanan, A.; Yang, Q.; Radha, B.; Taniguchi, T.; Watanabe, K.; Gomila, G.; Novoselov, K. S.; Geim, A. K. Anomalously Low Dielectric Constant of Confined Water. *Science* **2018**, *360*, 1339−1342.
(94) Karlberg, G.; Rossmeisl, J.; Nørskov, J. K. Estimations of Electric Field Effects on the Oxygen Reduction Reaction Based on the Density Functional Theory. *Phys. Chem. Chem. Phys.* **2007**, *9*, 5158−5161.
(95) Morikawa, K.; Kazoe, Y.; Mawatari, K.; Tsukahara, T.; Kitamori, T. Dielectric Constant of Liquids Confined in the Extended Nanospace Measured by a Streaming Potential Method. *Anal. Chem.* **2015**, *87*, 1475−1479.
(96) Schlaich, A.; Knapp, E. W.; Netz, R. R. Water Dielectric Effects in Planar Confinement. *Phys. Rev. Lett.* **2016**, *117*, 048001.
(97) Bard, A. J.; Faulkner, L. R.; Leddy, J.; Zoski, C. G. *Electrochemical Methods: Fundamentals and Applications*; Wiley: New York, 1980; Vol. *2*.
(98) Bockris, *Modern Electrochemistry 2A*; Kluwer Academic Publishers: Boston, 2002; Vol. *86*; pp 911−916.
(99) Garza, A.; Bell, A. T.; Head-Gordon, M. On the Mechanism of CO2 Reduction at Copper Surfaces: Pathways to C2 Products. *ACS Catal.* **2018**, *8*, 1490.
(100) Formaro, L.; Trasatti, S. Capacitance Measurements on Platinum Electrodes for the Estimation of Organic Impurities in Water. *Anal. Chem.* **1968**, *40*, 1060−1067.
(101) Filhol, J.-S.; Doublet, M.-L. Conceptual Surface Electrochemistry and New Redox Descriptors. *J. Phys. Chem. C* **2014**, *118*, 19023−19031.
(102) Rossmeisl, J.; Skúlason, E.; Björketun, M. E.; Tripkovic, V.; Nørskov, J. K. Modeling the Electrified Solid-Liquid Interface. *Chem. Phys. Lett.* **2008**, *466*, 68−71.
(103) Henkelman, G.; Jónsson, H. A Dimer Method for Finding Saddle Points on High Dimensional Potential Surfaces Using Only First Derivatives. *J. Chem. Phys.* **1999**, *111*, 7010−7022.
(104) Henkelman, G.; Uberuaga, B. P.; Jónsson, H. Climbing Image Nudged Elastic Band Method for Finding Saddle Points and Minimum Energy Paths. *J. Chem. Phys.* **2000**, *113*, 9901−9904.
(105) Henkelman, G.; Jónsson, H. Improved Tangent Estimate in the Nudged Elastic Band Method for Finding Minimum Energy Paths and Saddle Points. *J. Chem. Phys.* **2000**, *113*, 9978−9985.
(106) Singh, M. R.; Goodpaster, J. D.; Weber, A. Z.; Head-Gordon, M.; Bell, A. T. Mechanistic Insights Into Electrochemical Reduction of CO2 Over Ag Using Density Functional Theory and Transport Models. *Proc. Natl. Acad. Sci. U. S. A.* **2017**, *114*, E8812−E8821.
(107) Liu, L.; Liu, C. Origin of the Overpotentials for HCOO- and CO Formation in the Electroreduction of CO_2 on Cu (211): The Reductive Desorption Processes Decide. *Phys. Chem. Chem. Phys.* **2018**, *20*, 5756−5765.
(108) Kling, M. F.; Vrakking, M. J. Attosecond Electron Dynamics. *Annu. Rev. Phys. Chem.* **2008**, *59*, 463−492.
(109) Marcus, R. A. On the Theory of Oxidation-Reduction Reactions Involving Electron Transfer. I. *J. Chem. Phys.* **1956**, *24*, 966−978.
(110) Marcus, R. On the Theory of Electrochemical and Chemical Electron Transfer Processes. *Can. J. Chem.* **1959**, *37*, 155−163.
(111) Mayer, J. M. Simple Marcus-Theory-Type Model for Hydrogen-Atom Transfer/Proton-Coupled Electron Transfer. *J. Phys. Chem. Lett.* **2011**, *2*, 1481−1489.
(112) Atkins, P.; de Paula, J. *Physical Chemistry*; W.H. Freeman and Company: Oxford, 2006.
(113) Einstein, A. Über die von der Molekularkinetischen Theorie der Wärme Geforderte Bewegung von in Ruhenden Flüssigkeiten Suspendierten Teilchen. *Ann. Phys.* **1905**, *322*, 549−560.
(114) Bird, R.; Stewart, W.; Lightfoot, E. *Transport Phenomena*; Wiley: New York, 2007; p 780.
(115) Grün, F.; Jardat, M.; Turq, P.; Amatore, C. Relaxation of the Electrical Double Layer After an Electron Transfer Approached by Brownian Dynamics Simulation. *J. Chem. Phys.* **2004**, *120*, 9648−9655.
(116) Marković, N.; Grgur, B.; Ross, P. N. Temperature-Dependent Hydrogen Electrochemistry on Platinum Low-Index Single-Crystal Surfaces in Acid Solutions. *J. Phys. Chem. B* **1997**, *101*, 5405−5413.
(117) Robinson, R. A.; Stokes, R. H. *Electrolyte Solutions*, 2nd ed.; Butterworth & Co Publishers Ltd: London, 1965.
(118) Perdew, J. P.; Schmidt, K. Jacob's Ladder of Density Functional Approximations for the Exchange-Correlation Energy. *AIP Conf. Proc.* **2001**, *577*, 1.
(119) Greeley, J.; Jaramillo, T. F.; Bonde, J.; Chorkendorff, I.; Nørskov, J. K. Computational High-Throughput Screening of Electrocatalytic Materials for Hydrogen Evolution. *Nat. Mater.* **2006**, *5*, 909.
(120) Rossmeisl, J.; Logadottir, A.; Nørskov, J. K. Electrolysis of Water on (Oxidized) Metal Surfaces. *Chem. Phys.* **2005**, *319*, 178−184.
(121) Greeley, J.; Stephens, I.; Bondarenko, A.; Johansson, T. P.; Hansen, H. A.; Jaramillo, T.; Rossmeisl, J.; Chorkendorff, I.; Nørskov, J. K. Alloys of Platinum and Early Transition Metals As Oxygen Reduction Electrocatalysts. *Nat. Chem.* **2009**, *1*, 552.
(122) Stamenkovic, V.; Mun, B. S.; Mayrhofer, K. J.; Ross, P. N.; Markovic, N. M.; Rossmeisl, J.; Greeley, J.; Nørskov, J. K. Changing the Activity of Electrocatalysts for Oxygen Reduction by Tuning the Surface Electronic Structure. *Angew. Chem.* **2006**, *118*, 2963−2967.
(123) Zhang, J.; Vukmirovic, M. B.; Xu, Y.; Mavrikakis, M.; Adzic, R. R. Controlling the Catalytic Activity of Platinum-Monolayer Electrocatalysts for Oxygen Reduction With Different Substrates. *Angew. Chem.* **2005**, *117*, 2170−2173.
(124) Dickens, C. F.; Nørskov, J. K. A Theoretical Investigation into the Role of Surface Defects for Oxygen Evolution on RuO2. *J. Phys. Chem. C* **2017**, *121*, 18516−18524.
(125) Man, I. C.; Su, H.-Y.; Calle-Vallejo, F.; Hansen, H. A.; Martínez, J. I.; Inoglu, N. G.; Kitchin, J.; Jaramillo, T. F.; Nørskov, J. K.; Rossmeisl, J. Universality in Oxygen Evolution Electrocatalysis on Oxide Surfaces. *ChemCatChem* **2011**, *3*, 1159−1165.
(126) Kirk, C.; Chen, L. D.; Siahrostami, S.; Karamad, M.; Bajdich, M.; Voss, J.; Nørskov, J. K.; Chan, K. Theoretical Investigations of the Electrochemical Reduction of CO on Single Metal Atoms Embedded in Graphene. *ACS Cent. Sci.* **2017**, *3*, 1286.

DOI: 10.1021/acscatal.8b02793
ACS Catal. 2019, 9, 920−931